

# High permittivity short-range orthorhombic Q phase in CaTiO3 modified NaNbO3 ceramics

ZUBAIRI, Hareem, WASIM, Muhammad, LIU, Yang, CHEN, Ying, LU, Zhilun

<a href="http://orcid.org/0000-0002-9967-5221">http://orcid.org/0000-0002-9967-5221</a>, XU, Diming, FETEIRA, Antonio

<a href="http://orcid.org/0000-0001-8151-7009">http://orcid.org/0000-0001-8151-7009</a>, HERLIHY, Anna

<a href="http://orcid.org/0000-0002-2851-3911">http://orcid.org/0000-0002-2851-3911</a> and WANG, Ge

<a href="http://orcid.org/0000-0003-1842-8067">http://orcid.org/0000-0003-1842-8067</a>

Available from Sheffield Hallam University Research Archive (SHURA) at:

https://shura.shu.ac.uk/36409/

This document is the Published Version [VoR]

## Citation:

ZUBAIRI, Hareem, WASIM, Muhammad, LIU, Yang, CHEN, Ying, LU, Zhilun, XU, Diming, FETEIRA, Antonio, HERLIHY, Anna and WANG, Ge (2025). High permittivity short-range orthorhombic Q phase in CaTiO3 modified NaNbO3 ceramics. Ceramics International, 51 (28), 59862-59867. [Article]

# Copyright and re-use policy

See <a href="http://shura.shu.ac.uk/information.html">http://shura.shu.ac.uk/information.html</a>

ELSEVIER

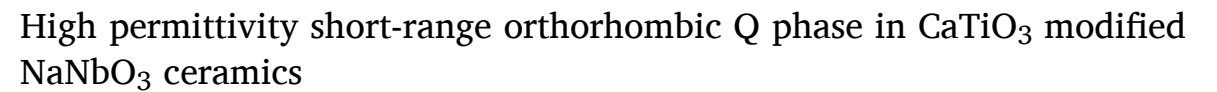
Contents lists available at ScienceDirect

## Ceramics International

journal homepage: www.elsevier.com/locate/ceramint



#### Short communication





- <sup>a</sup> Department of Materials, University of Manchester, Manchester, M13 9PL, UK
- <sup>b</sup> School of Engineering and Built Environment, Sheffield Hallam University, Sheffield, S1 1WB, UK
- ESchool of Chemical and Process Engineering, University of Leeds, Leeds, LS2 9JT, UK
- d Multifunctional Materials and Structures, Key Laboratory of the Ministry of Education & International Center for Dielectric Research, School of Electronic Science and Engineering, Xi'an Jiaotong University, Xi'an, 710049, China
- <sup>e</sup> Diamond Light Source, Harwell Campus, Oxfordshire, OX11 0DE, UK

#### ARTICLE INFO

Handling Editor: P. Vincenzini

Keywords: Lead-free Relaxor ferroelectric NaNbO<sub>3</sub> High permittivity

#### ABSTRACT

The structural evolution and electrical behaviour of (1-x) NaNbO $_3$ -xCaTiO $_3$  (NN-CT) ceramics were investigated in this study. X-ray diffraction and full-pattern Rietveld refinement confirm that CT incorporation disrupts the long-range antipolar orthorhombic *Pbcm* phase. The dielectric permittivity peak shifts to lower temperatures as the CT concentration increases. The highest permittivity of 2365 was obtained for x=0.15 at room temperature. Synchrotron X-ray scattering coupled with pair distribution function (PDF) analysis reveals the existence of a short-range ordered polar orthorhombic  $P2_1ma$  (Q) phase with a correlation length of approximately 5 nm. A slim ferroelectric polarisation-electric field (P-E) loop, consistent with short-range ordered behaviour, was obtained in the NN-0.15CT, yielding an enhanced recoverable energy density by over 300 % at 150 kV cm<sup>-1</sup> compared to pure NN. These findings establish the role of CT doping in modifying structural and dielectric properties, contributing to the understanding of crystal symmetry evolution and its impact on the dielectric response of this promising, environmentally friendly lead-free perovskite oxide for high-performance dielectric applications.

## 1. Introduction

Sodium niobate (NaNbO<sub>3</sub>, NN) is a perovskite oxide that undergoes multiple phase transitions, a versatile system for functional applications such as dielectric capacitors, piezoelectrics, and antiferroelectric energy storage devices [1–4]. Among the key goals for a sustainable environment, the demand for lead-free, high-performance dielectric materials has been modified due to the increasing need for efficient energy storage technologies [5]. NN has gained attention for its high intrinsic breakdown strength [6] (high band gap $\sim$ 3.4 eV) [7,8], low dielectric loss [9, 10], and complex polar ordering, compared to other studied ceramics like Na<sub>0.5</sub>Bi<sub>0.5</sub>TiO<sub>3</sub>, K<sub>0.5</sub>Na<sub>0.5</sub>NbO<sub>3</sub>, BaTiO<sub>3</sub>, making it a strong alternative to lead-based ferroelectrics for capacitor applications. Additionally, NN-based ceramics exhibit a broad range of polar and antipolar phases as the B-site contains a highly polarisable d<sup>0</sup> ion, which is often linked to octahedral distortions [11,12] with nearly equivalent free energies [1,

13,14], which can be modified through doping and processing to enhance their dielectric and energy density performance [15]. These structural instabilities can effectively disrupt long-range polar order to facilitate a short-range relaxor behaviour [16,17].

At room temperature (RT), NN generally exists in an antiferroelectric (AFE) P-phase (Pbcm),  $\sqrt{2}a \times \sqrt{2}a \times 4a$  [8,9]. Upon heating, NN undergoes a series of tilt transitions. For example, at 360 °C, the P phase transforms into the R-phase (orthorhombic, Pnma),  $\sqrt{2}a \times 6a \times \sqrt{2}a$ , followed by the S-phase (orthorhombic, Pnma) at 480 °C. It then further transitions into higher-temperature paraelectric phases (T1 (Orthorhombic, Ccmm), T2 (Tetragonal, F4/mmb), and U (cubic,  $Pm\overline{3}m$ ) above 520 °C [10,12]. While these transitions are well-observed in NN, the key structural transformation in NN occurs under an application of an external electric field, where the AFE-P phase is irreversibly transformed into the FE Q-phase ( $P2_1ma$ ,  $P2_1ma$ ,  $P2_1ma$ ) at  $P2_1ma$ ,  $P3_1ma$ , P

E-mail address: ge.wang@manchester.ac.uk (G. Wang).

 $<sup>^{\</sup>ast}$  Corresponding author.

polarisation switching becomes possible, yet structural features such as antipolar displacements and octahedral tilt patterns characteristic of the AFE P-phase are partially retained [18]. Phase stability and associated dielectric behaviour are highly dependent on the ceramic composition, grain size, processing conditions, and applied field [19].

To quantify the energy density performance of a dielectric ceramic, the discharge energy density ( $W_{rec}$ ) is calculated using  $W_{rec}$  =  $\int_{P_r}^{P_{max}} E dP$ , where  $P_{max}$  is the maximum polarisation under the applied field, Pr is the remnant polarisation, and E is the electric field, respectively [20]. Many studies have focused on the structural modification and phase transition behaviour of NN-based ceramics, such as NN-SrTiO<sub>3</sub> (NN-ST), where the relaxor phase was obtained for optimisation of the Wrec of ceramic capacitors. For example, relaxor ferroelectric ceramics based on NN-0.10ST and NN-0.15ST have been reported in the literature, with a permittivity value of  $\sim$ 1000 and a  $W_{rec}$ of 1.5 J cm<sup>-3</sup> at 140 kV cm<sup>-1</sup> [21–23]. However, incorporating CaTiO<sub>3</sub> (CT) into NN has received less attention in the literature, but is expected to have a pronounced impact due to the even smaller ionic radii of Ca (1.34 Å) compared to Sr (1.44 Å) [24]. Although CT processes low dielectric loss ( $\sim$ 0.0005 at 1 kHz) and a wide bandgap ( $\sim$ 3.4 eV) [25], its low permittivity of ~170 restricts CT from being a promising candidate for high-voltage, high-discharge energy/power capacitors. Both NN and CT have the same orthorhombic framework (e.g., Pbcm for NN and Pbnm for CT) with a complex octahedra tilting structure (e.g., a a c<sup>+</sup>). Incorporating CT into NN, therefore, allows for inducing more structural disorder compared to NN-ST, which is ideal for creating a short-range relaxor [26,27].

In this work, we synthesised a series of ceramic compositions based on (1-x) NN-xCT (x = 0.00–0.20). The substitution of  ${\rm Ca}^{2+}$  for  ${\rm Na}^+$  and  ${\rm Ti}^{4+}$  for  ${\rm Nb}^{5+}$  introduces local distortions due to size mismatch and charge imbalance, modifying the crystal lattice through strain and defect formation [10]. This aims to suppress long-range ferroelectric order and facilitate the formation of polar nanoregions (PNRs), which are characteristic of relaxor materials [28,29]. The study is focused on understanding the phase transition behaviour from a long-range ferroelectric to a short-range relaxor ferroelectric phase and the role of polar nanoregions contributing to dielectric behaviour. This work also demonstrates fundamental insights into the development of new lead-free dielectrics for high-voltage, high-discharge-energy-density capacitors.

## 2. Materials and methods

The (1–x) NN–xCT ceramics (x = 0.00–0.20) were prepared using a conventional solid-state reaction method. Analytical-grade Na<sub>2</sub>CO<sub>3</sub> ( $\geq$ 99.9 %, Sigma Aldrich, USA), Nb<sub>2</sub>O<sub>5</sub> (99.9 %, Sigma Aldrich, China), CaCO<sub>3</sub> ( $\geq$ 99.0 %, Sigma Aldrich, Germany), and TiO<sub>2</sub> ( $\geq$ 99.9 %, Sigma

Aldrich, Japan) powders were dried to remove moisture, weighed in stoichiometric ratios, and ball-milled in propan-2-ol for 24 h. The dried powders were calcined at 900  $^{\circ}$ C for 5 h, followed by 2nd ball-milling to get homogenous powders, then mixed with 1 wt% PVA binder, and pressing into 10 mm-diameter ceramic pellets under 150–180 MPa. After the binder removal stage at 550  $^{\circ}$ C for 2 h, the ceramic pellets were sintered at 1330–1400  $^{\circ}$ C for 2 h with a heating rate of 3  $^{\circ}$ C per minute, resulting in dense ceramics with relative densities above 93 %.

Sintered pellets for electrical measurements were electrode with silver paste and fired at 500  $^{\circ}\text{C}$  for 30 min. Temperature-dependent dielectric properties were recorded in the temperature range from 25 to 550 °C, at frequencies of 1, 10, and 100 kHz using an LCR meter (HP 4284A Precision LCR Meter, Agilent Technologies, USA). Polarisationelectric field (P-E) loops were measured on 0.1-0.2 mm thick pellets with 1 mm<sup>2</sup> gold electrode area using a TF Analyser 2000 (aixACCT, Germany) at 1Hz under silicone oil. X-ray diffraction (XRD) was performed on crushed sintered ceramics using Cu K $\alpha$  radiation ( $\lambda = 1.5406$ Å) with a PANalytical X'Pert PRO diffractometer to analyse phase evolution and lattice distortions. Ceramic samples for microstructural analysis were prepared by grinding, polishing, and thermal etching at 70 % of the sintering temperature for 10 min. The scanning electron microscopy (SEM) imaging was conducted using FE-SEM (Quanta 250, JEOL, Japan). Transmission electron microscopy (TEM) samples were prepared using a focused ion beam (FIB, FEI Quanta 3D, The Netherlands) and analysed using TEM (FEI Tecnai G2-20, The Netherlands). Bulk ceramic specimens for the synchrotron X-ray scattering experiment were crushed into fine powders, thermally annealed at 600 °C for 4 h, and passed through a fine sieve. The sieve powders were then loaded into 1 mm diameter borosilicate capillaries with a packing fraction of greater than 80 % and sealed. Synchrotron X-ray total scattering data were collected at beamline I15-1, Diamond Light Source, with a wavelength ( $\lambda$ ) of 0.161669 Å. During measurement, the samples were continuously spun to ensure uniform exposure, with data collected using a PerkinElmer XRD 4343CT detector. The obtained X-ray total scattering data were converted into X-ray pair distribution function (XPDF) data using GudrunX and a Q-range of 0.5–25  $\text{Å}^{-1}$ , followed by 'box-car' analysis at ranges of 2–12 Å, 2–22 Å, 2–32 Å, 2–42 Å and 2–52 Å using PDFgui to evaluate local structural distortions over various rranges from 2 to 52 Å.

## 3. Results

The XRD patterns of (1-x)NN-xCT ceramics are shown in Fig. 1a. Single-phase perovskite structure was obtained without any secondary phases, indicating that  $Ca^{2+}$  and  $Ti^{4+}$  are incorporated successfully into the NN lattice [30]. With increasing the CT content, the doublet  $\{200\}_{DC}$ 

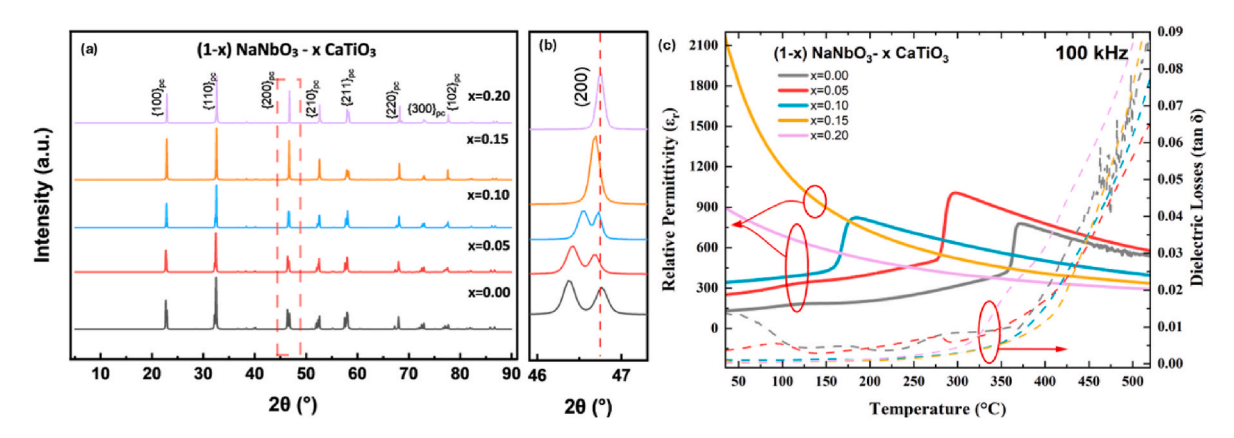


Fig. 1. (a) XRD patterns (b) enlarged view for  $\{200\}_{pc}$  reflection (c) Dielectric permittivity ( $\epsilon_r$ ) and loss ( $\tan\delta$ ) as a function of temperature at 100 kHz for (1-x) NN–xCT ceramics.

(pc refers to pseudocubic) peak merged into a single peak whilst shifting to higher 20 (Fig. 1b), suggesting a change in crystal symmetries, accompanied by a reduction in unit cell volume due to the substitution of  $Ca^{2+}$  (1.34 Å, CN = 12) for  $Na^{+}$  (1.39 Å, CN = 12) at the A-site and  $Ti^{4+}$  (0.61 Å, CN = 6) for  $Nb^{5+}$  (0.64 Å, CN = 6) at the B-site [24]. Full-pattern Rietveld refinement, Fig. S1, for x = 0.15 (Supplementary data), was performed in TOPAS using a few structures and space groups, including orthorhombic Pbcm, Pbnm, and P21ma, Rhombohedral R3m, and Cubic Pm  $\overline{3}$  m. The best-refined structure obtained for x = 0.00 is orthorhombic *Pbcm*. Superlattice reflections (between  $2\theta = 36^{\circ}-41^{\circ}$ ) remain for all compositions, such as {102}<sub>pc</sub> and {240}<sub>pc</sub>, Fig. S2 (Supplementary data). The best-refined structure of x = 0.15 is obtained using P2<sub>1</sub>ma. Moreover, SEM morphology, Fig. S3 (Supplementary data), of (1-x)NN-xCT ceramics reveals a dense microstructure (>93 %) with uniform grain morphology and no observable secondary phases, further reinforcing the phase purity observed in XRD. A gradual decrease in average grain size is observed with increasing CT content, reducing from  ${\sim}6.8\pm0.2~\mu\text{m}$  at x=0.00 to  ${\sim}4.9\pm0.3~\mu\text{m}$  at x=0.20. The average grain size for x = 0.15 is found to be approximately 5.2  $\pm$ 0.3 μm.

The temperature-dependent dielectric properties for all compositions of the (1-x) NN-xCT ceramics are presented in Fig. 1c and Fig. S4 (Supplementary data). With increasing CT concentration to x = 0.05 and 0.10, the dielectric peak shifts progressively to lower temperatures, subject to pseudo-cubic structure formation, which is the associated P to R AFE phase transition, from approximately 360 °C down to 190 °C with slightly increased permittivity at RT. For x = 0.15 and 0.20, no sharp dielectric peak is observed above RT, with a permittivity of 2365 obtained at x = 0.15, the highest among all NN-based compositions reported here. High permittivity quasi-linear dielectric has been recently reported by Wang and Reaney as one of the most promising strategies for realising giant discharge energy density [31]. The dielectric loss at RT is found to be decreased from 0.014 (tan  $\delta = 1.4$  %) for x = 0.00 to 0.002 (tan  $\delta = 0.2$  %) for x = 0.15, which is significantly below the values typically reported for other NN-based ceramics (tan  $\delta < 1\,$  %) in the literature [22,32,33]. This is very important for a high-voltage ceramic capacitor with low self-heating during charging-discharging cyclic operation. Compared with the widely studied NBT-based systems, which commonly exhibit higher dielectric losses at RT (tan  $\delta > 1$  %), NN-CT demonstrates a markedly superior low-loss performance [2,34,35].

The local structural behaviour of NN-0.15CT ceramics was investigated using TEM and XPDF (Fig. 2). The dark field image (Fig. 2a) obtained from the <101> zone axis shows ferroelastic domain walls, similar to the NN-ST based ceramics [31]. The selected area electron diffraction (SAED) patterns along <101> showed a doubling of periodic superlattice reflections  $\frac{1}{2}$ <hkl>, confirming the presence of the Q phase

at the nanoscale. Different from NN-ST, both CT and NN have the same tilt structure of a a c + therefore, the Q phase is favourable to be stabilised, along with the formation of ferroelastic walls since the dielectric peak is below RT, Fig. 1c [36,37]. This short-range Q phase was then further studied using XPDF, Fig. 2b, and Fig. S5 (Supplementary data). The XPDF patterns of (1-x) NN-xCT ceramics (x = 0.05-0.20) were refined using "box-car" refinement to investigate local structural distortions and polar correlation. Multiple structural models, including orthorhombic *Pbcm*, *Pnma*, and *P21ma*, were used to refine, with the best fits obtained using the P21ma space group across all r-ranges. At very short length scales (r < 6 Å), the structural fitting shows deviations from the P21ma model, similar to a previous report of NN in a neutron scattering study, suggesting a chemical disorder behaviour [38,39]. The local structure was fitted well with orthorhombic P21ma, indicating a polar correlation length of approximately 5 nm.

The local crystallographic information (2–52 Å), obtained from the 'box-car' XPDF analysis, was presented in Fig. 3. The general trend across all compositions is a decrease in lattice parameter a but an increase in lattice parameter b/c, indicating enhancement of the local structural distortion. These distortions are found to decrease with increasing box range. The lattice parameters obtained at the largest box range of 2–52 Å are closer to the crystallographic information obtained from Rietveld refinement, Table S1 (Supplementary data). This strong local distorted structure reveals the existence of short-range orthorhombic symmetries of 10–50 Å within a pseudo-orthorhombic matrix, which could be responsible for the high permittivity value at RT.

The unipolar P-E loop and calculated energy density performance of the relaxor phase NN-0.15CT are shown in Fig. 4a. The slim P-E loop gives a  $W_{rec}$  of 0.7 J cm<sup>-3</sup> with efficiency ( $\eta$ ) of 82 % at an electric field of 150 kV cm<sup>-1</sup>, significantly enhanced from undoped NN (0.05 J cm<sup>-3</sup> at the same field, Fig. S6 (Supplementary data), attributed mainly to the short-range ferroelectric (relaxor-like) state [40,41]. Both P and  $W_{rec}$ values at 150 kV cm<sup>-1</sup> obtained in the NN-0.15CT are found to be higher than other NN-based counterparts, such as  $0.88NN-0.12Bi(Sn_{0.5}Ni_{0.5})O_3$  $(W_{rec} \approx 0.56 \text{ J cm}^{-3})$  [42], mainly due to the high permittivity value. Another important energy density performance index, the polarisation max and increments (dP/dE), were also evaluated in this study, as shown in Fig. 4b [43-45]. The dP/dE was found to decrease gradually from approximately 0.086 to 0.065 as the electric field increased, indicating a relaxor unsaturation state and a deviation from ideal quasi-linear dielectrics. This behaviour arises from short-range polar correlations and local structural distortions which collectively limit the linear polarisation response. Further compositional modification is still required in future work to further reduce polar coupling (down to cell-to-cell only) by inducing more complex chemical and tilting disorders in the ceramics.

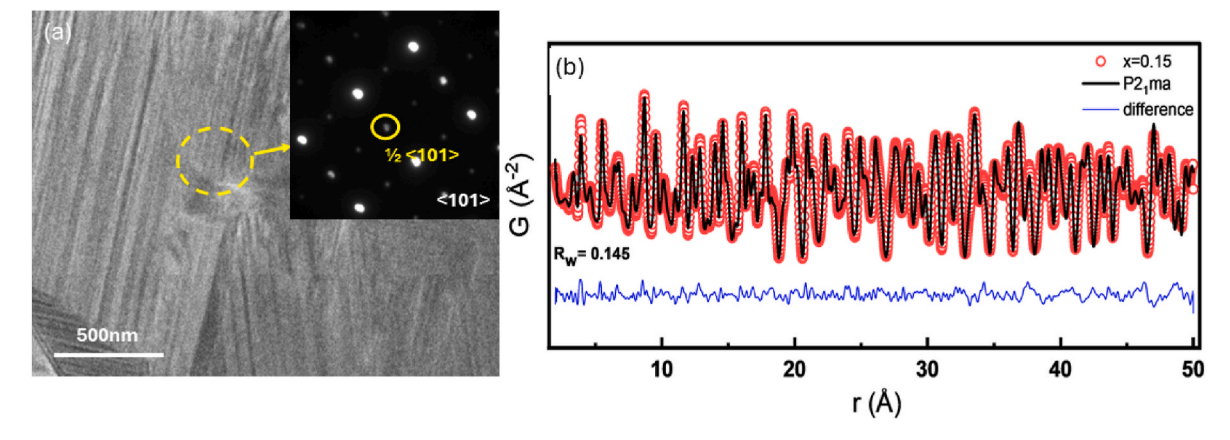


Fig. 2. (a) TEM dark-field images and SAED patterns of x = 0.15, confirming Q-phase formation with 1/2 (hkl) superlattice reflections (b) Room-temperature XPDF data fitted using the  $P2_1ma$  model, confirming short-range structural distortions.

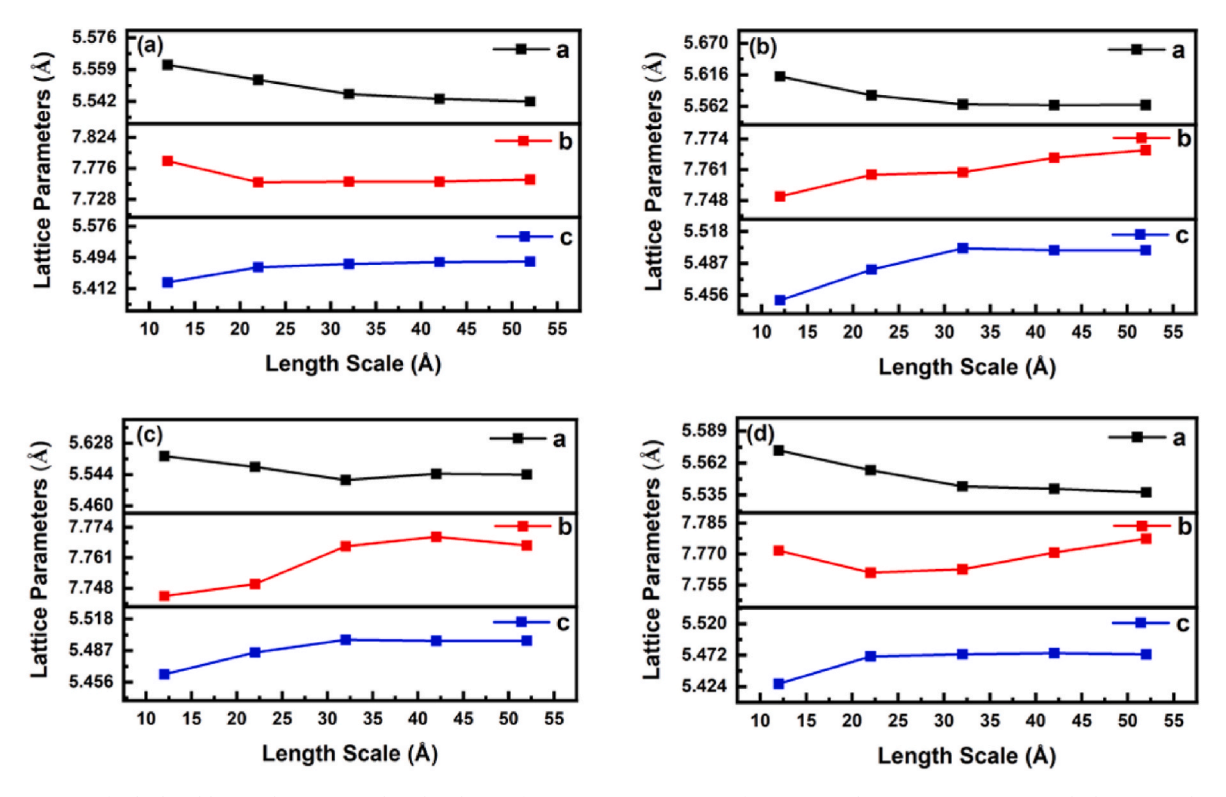


Fig. 3. Comparison of calculated lattice distortion within the planes of (1-x) NN-x CT ceramics for (a) 0.05, (b) 0.10, (c) x = 0.15, and (d) 0.20, as determined by analysis at different length scales of XPDF data.

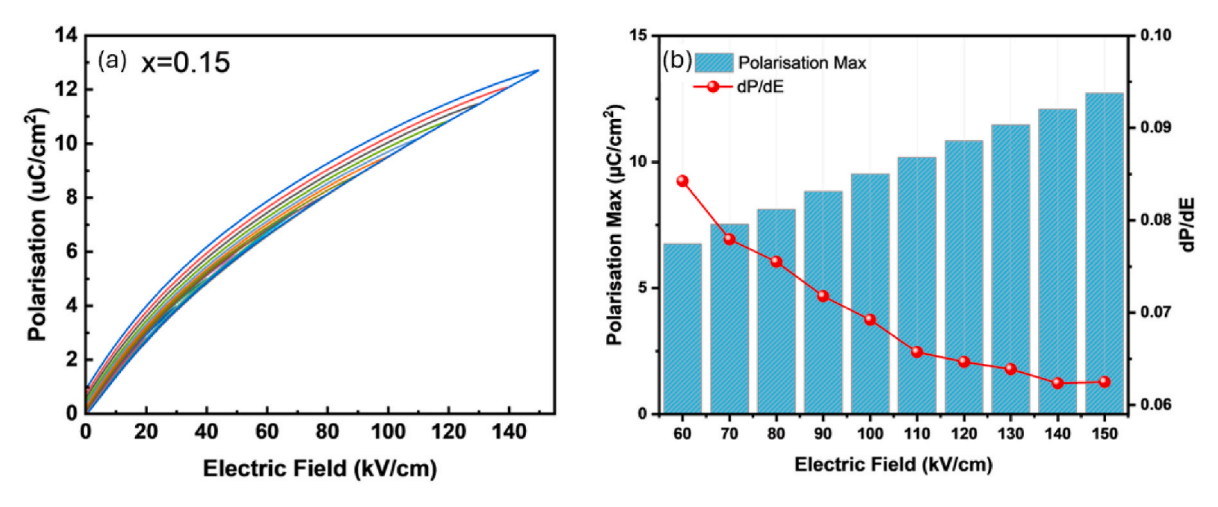


Fig. 4. (a) Unipolar P-E loops of x = 0.15 (b) Polarisation max and dP/dE ratio vs. electric field as derived from (a).

## 4. Conclusion

The structural evolution and electrical properties of (1-x) NN–xCT ceramics were investigated in this study. The changes in the macroscopic structure from long-range to short-range orthorhombic were revealed under XRD as increasing CT concentration. Short-range polar Q phase was further examined under TEM and XPDF in the 0.85NN-0.15CT ceramics. The phase transition temperature obtained from dielectric curves is found to shift toward lower temperatures with enhanced permittivity. The highest permittivity of 2365 at RT was obtained with x=0.15, probably due to the highly distorted polar phase at the local scale. A slim P-E loop was obtained for x=0.15, along with a reduction in the dP/dE value, indicating an unsaturated relaxor-like behaviour. These findings provide key insights into inducing a short-

range state for optimisation of discharge energy density in the NN-CT ceramic solid solution.

#### CRediT authorship contribution statement

Hareem Zubairi: Writing – original draft, Visualization, Software, Methodology, Investigation, Formal analysis, Data curation, Conceptualization. Muhammad Wasim: Data curation. Yang Liu: Data curation. Ying Chen: Data curation. Zhilun Lu: Data curation. Diming Xu: Data curation. Antonio Feteira: Data curation. Anna Herlihy: Data curation. Ge Wang: Writing – review & editing, Validation, Supervision, Investigation, Conceptualization.

#### Declaration of competing interest

The authors declare that they have no known competing financial interests or personal relationships that could have appeared to influence the work reported in this paper.

#### Acknowledgements

The authors gratefully acknowledge the financial support from the Dean's PhD Scholarship by the University of Manchester and the Dame Kathleen Ollerenshaw Fellowship. We would also like to acknowledge the funding support through EPSRC grant (EP/Z536003/1) and Diamond Light Source (proposal no CY34380) for accessing the synchronous experiment. We also thank Prof Ian M Reaney from the University of Sheffield for the useful discussion.

#### Appendix A. Supplementary data

Supplementary data to this article can be found online at https://doi.org/10.1016/j.ceramint.2025.10.204.

#### References

- Z. Chen, et al., Phase engineering in NaNbO3 antiferroelectrics for high energy storage density, Journal of Materiomics 8 (4) (2022/7//2022) 753–762, https://doi.org/10.1016/J.JMAT.2022.03.004.
- [2] W. Cheng, L. Xiaojie, High energy storage properties of 0.94Bi<sub>0.5</sub>Na<sub>0.5</sub>TiO<sub>3</sub>-0.06BaTiO<sub>3</sub> ceramics by incorporating Sr<sub>0.8</sub>Bi<sub>0.170.1</sub>Ti<sub>0.8</sub>Zr<sub>0.2</sub>O<sub>2.95</sub>, Microstructures 3 (3) (2023) 2023023, https://doi.org/10.20517/microstructures.2023.04.
- [3] J. Yin, et al., Conformable shear mode transducers from lead-free piezoelectric ceramic coatings: an innovative ultrasonic solution for submerged structural health monitoring, Adv. Funct. Mater. 34 (32) (2024/08/01 2024) 2401544, https://doi. org/10.1002/adfm.202401544.
- [4] J. Yin, S. Chen, V.K. Wong, K. Yao, Thermal sprayed lead-free piezoelectric ceramic coatings for ultrasonic structural health monitoring, IEEE Trans. Ultrason. Ferroelectrics Freq. Control 69 (11) (2022) 3070–3080, https://doi.org/10.1109/ TUFFC.2022.3176488.
- [5] J. Yin, et al., Deciphering the atomic-scale structural origin for large dynamic electromechanical response in lead-free Bi<sub>0.5</sub>Na<sub>0.5</sub>TiO<sub>3</sub>-based relaxor ferroelectrics, Nat. Commun. 13 (1) (2022/10/25 2022) 6333, https://doi.org/10.1038/s41467-022.34062-6.
- [6] N. Bein, et al., Fermi energy, electrical conductivity, and the energy gap of NaNbO<sub>3</sub>, Phys. Rev. Mater. 6 (8) (2022) 084404, https://doi.org/10.1103/ PhysRevMaterials.6.084404.
- Z. Lu, et al., Mechanism of enhanced energy storage density in AgNbO3-based leadfree antiferroelectrics, Nano Energy 79 (2021) 105423, https://doi.org/10.1016/J. NANOEN.2020.105423, 105423, 2021/1//.
- [8] N. Luo, et al., Design for high energy storage density and temperature-insensitive lead-free antiferroelectric ceramics, J. Mater. Chem. C 7 (17) (2019) 4999–5008, https://doi.org/10.1039/C8TC06549G.
- [9] Z. Pan, L. Yao, G. Ge, B. Shen, J. Zhai, High-performance capacitors based on NaNbO<sub>3</sub> nanowires/poly(vinylidene fluoride) nanocomposites, J. Mater. Chem. A 6 (30) (2018/7//2018) 14614–14622, https://doi.org/10.1039/C8TA03084G.
- [10] A. Xie, et al., NaNbO<sub>3</sub>-CaTiO<sub>3</sub> lead-free relaxor antiferroelectric ceramics featuring giant energy density, high energy efficiency and power density, Chem. Eng. J. 429 (2022) 132534, https://doi.org/10.1016/J.CEJ.2021.132534, 132534, 2022/2//.
- [11] G. Shirane, R. Newnham, R. Pepinsky, Dielectric properties and phase transitions of NaNbO<sub>3</sub> and (Na,K)NbO<sub>3</sub>, Phys. Rev. 96 (3) (1954) 581–588, https://doi.org/ 10.1103/PhysRev.96.581.
- [12] M. Ahtee, A.M. Glazer, H.D. Megaw, The structures of sodium niobate between 480° and 575°c, and their relevance to soft-phonon modes, Philos. Mag. 26 (4) (1972) 995–1014, https://doi.org/10.1080/14786437208226972.
- [13] S. Zhang, W. Li, Y. Zhang, X. Tang, Y. Jiang, X. Guo, Excellent energy density and power density achieved in NaNbO<sub>3</sub>-based relaxor ferroelectric ceramics, Mater. Sci. Eng., B 299 (2024) 117025, https://doi.org/10.1016/J.MSEB.2023.117025, 117025, 2024/1//.
- [14] H. Li, et al., Dielectric temperature stability and energy storage performance of NBT-based lead-free ceramics for Y9P capacitors, World ScientificH Li, S Zhou, J Zhao, T Yan, Y Du, H Zhou, Y Pu, D Wang, Journal of Advanced Dielectrics 13 (1) (2023) 2242007, https://doi.org/10.1142/S2010135X22420073, 2242007, 2023/ 2//.
- [15] T.E. Hooper, D.C. Sinclair, Structural, dielectric, and conduction behaviour of Asite deficient  $Sr_xNa_{1-2x}NbO_3$  ceramics, J. Mater. Chem. C 12 (33) (2024) 12992–13001, https://doi.org/10.1039/D4TC02433H, 10.1039/D4TC02433H.
- [16] L. Oliveira, et al., Coupled local residual shear and compressive strain in NaNbO<sub>3</sub> ceramics under cooling, Acta Mater. 266 (2024/03/01/2024) 119640, https://doi.org/10.1016/j.actamat.2023.119640.

- [17] H. Zubairi, Yubo Zhu, Zhilun Lu, Ian M. Reaney, Ge Wang, Current development, optimisation strategies and future perspectives for lead-free dielectric ceramics in high field and high energy density capacitors, Chem. Soc. Rev. (2024), https://doi.org/10.1039/D4CS00536H
- [18] L. Eric Cross, Relaxor ferroelectrics, Ferroelectrics 76 (1) (1987) 241–267, https://doi.org/10.1080/00150198708016945.
- [19] H. Zhang, B. Yang, H. Yan, I. Abrahams, Isolation of a ferroelectric intermediate phase in antiferroelectric dense sodium niobate ceramics, Acta Mater. 179 (2019) 255–261, %@ 1359-6454.
- [20] Z. Lu, et al., Energy storage properties in Nd-doped AgNbTaO<sub>3</sub> lead-free antiferroelectric ceramics with Nb-site vacancies, Journal of Advanced Dielectrics 13 (1) (2023/02/01 2022) 2242006, https://doi.org/10.1142/ \$2010135X22420061
- [21] A. Xie, H. Qi, R. Zuo, Achieving remarkable amplification of energy-storage density in two-step sintered NaNbO $_3$ -SrTiO $_3$  antiferroelectric capacitors through dual adjustment of local heterogeneity and grain scale, ACS Appl. Mater. Interfaces 12 (17) (2020/4//2020) 19467–19475, https://doi.org/10.1021/ACSAMI.0C00831.
- [22] P. Nong, et al., Simultaneous enhancement of energy storage performance and thermal stability of NaNbO3-based ceramics via multi-scale modulation, Journal of Materiomics (2023), https://doi.org/10.1016/J.JMAT.2023.09.004, 2023/10.
- [23] K. Kusumoto, Dielectric and piezoelectric properties of NaNbO<sub>3</sub> BaTiO <sub>3</sub> SrTiO<sub>3</sub> ceramics, in: IEEE International Symposium on Applications of Ferroelectrics, 2007, pp. 686–687, https://doi.org/10.1109/ISAF.2007.4393370.
- [24] R.D. Shannon, urn:issn:0567-7394, Revised Effective Ionic Radii and Systematic Studies of Interatomic Distances in Halides and Chalcogenides, vol. 32, 1976/9// 1976, pp. 751–767, https://doi.org/10.1107/S0567739476001551, 5.
- [25] A. Krause, Ultrathin CaTiO<sub>3</sub> Capacitors: Physics and Application, 2014.
- [26] M. Xu, et al., 0.90(0.88NaNbO<sub>3</sub>-0.12Bi(Ni<sub>0.5</sub>Zr<sub>0.5</sub>)O<sub>3</sub>)-0.10CaTiO<sub>3</sub> lead-free dielectric ceramics with high energy storage properties, ACS Appl. Energy Mater. 6 (3) (2023) 1630–1638, https://doi.org/10.1021/ACSAEM.2C03520/SUPPL\_FILE/AE2C03520\_SI\_001.PDF, 2023/2.
- [27] P. Nong, et al., Inner mechanism of enhanced energy storage properties and efficiency for CaTiO<sub>3</sub> modified 0.92NaNbO<sub>3</sub>-0.08Bi(Mg<sub>0.5</sub>Ti<sub>0.5</sub>)O<sub>3</sub> lead-free ceramics, Electron. Mater. Lett. 1 (2023) 1–13, https://doi.org/10.1007/S13391-023-00434-3/FIGURES/11, 2023/5//.
- [28] H. Ghoudi, S. Chkoundali, Z. Raddaouic, A. Aydib, Structure properties and
- dielectric relaxation of Ca<sub>0.1</sub>Na<sub>0.9</sub>Ti<sub>0.1</sub>Nb<sub>0.9</sub>O<sub>3</sub> ceramic, RSC Adv. 9 (2019) 25358.

  [29] P. Palani, D. Fasquelle, A. Tachafine, A review on (Sr, Ca) TiO<sub>3</sub>-based dielectric materials: crystallography, recent progress and outlook in energy-storage aspects, J. Mater. Sci. 57 (26) (2022) 12279–12317.
- [30] S. Tripathi, D. Pandey, S.K. Mishra, P.S.R. Krishna, Morphotropic phase-boundary-like characteristic in a lead-free and non-ferroelectric (1-x) NaNbO<sub>3</sub> xCaTiO<sub>3</sub> system, Phys. Rev. B 77 (5) (2008) 052104, https://doi.org/10.1103/PhysRevB.77.052104.
- [31] X. Wang, et al., Lead-free high permittivity quasi-linear dielectrics for giant energy storage multilayer ceramic capacitors with broad temperature stability, Adv. Energy Mater. 14 (31) (2024/08/01 2024) 2400821, https://doi.org/10.1002/ aepm 202400821
- [32] Z. Peiyao, L. Longtu, W. Xiaohui, BaTiO<sub>3</sub>-NaNbO<sub>3</sub> energy storage ceramics with an ultrafast charge-discharge rate and temperature-stable power density, Microstructures 3 (1) (2023) 2023002, https://doi.org/10.20517/ microstructures.2022.21.
- [33] X. Mingzhao, et al., Optimizing the energy storage performance of NaNbO<sub>3</sub> ceramics by rare-earth-based composite perovskite Sm(Mg<sub>0.5</sub>Zr<sub>0.5</sub>)O<sub>3</sub> modification, Microstructures 3 (4) (2023) 2023034, https://doi.org/10.20517/microstructures 2023 19
- [34] L.N. Shi, Y.G. Wang, Z.H. Ren, A. Jain, S.S. Jiang, F.G. Chen, Significant improvement in electrical characteristics and energy storage performance of NBTbased ceramics, Ceram. Int. 48 (18) (2022/09/15/2022) 26973–26983, https:// doi.org/10.1016/j.ceramint.2022.06.009.
- [35] A. Zhang, et al., Significant improvement in energy storage for BT ceramics via NBT composition regulation, J. Alloys Compd. 968 (2023) 172255, https://doi. org/10.1016/J.JALLCOM.2023.172255, 172255, 2023/12//.
- [36] P.B. Groszewicz, et al., Reconciling local structure disorder and the relaxor state in (Bi<sub>1/2</sub>Na<sub>1/2</sub>)TiO<sub>3</sub>-BaTiO<sub>3</sub>, Sci. Rep. 6 (1) (2016/08/22 2016) 31739, https://doi. org/10.1038/srep31739.
- [37] J. Zuo, A. Xie, J. Liu, Y. Zhang, R. Zuo, Significantly enhanced energy-storage properties in NaNbO<sub>2</sub>-based relaxor ferroelectric ceramics via introducing a wide band-gap linear dielectric, Ceram. Int. 50 (4) (2024) 6332–6339, https://doi.org/ 10.1016/j.ceramint.2023.11.363.
- [38] Y. Yoneda, R. Aoyagi, D. Fu, Local structure analysis of NaNbO<sub>3</sub> and AgNbO<sub>3</sub> modified by li substitution, Jpn. J. Appl. Phys. 55 (10S) (2016/08/30 2016) 10TC04, https://doi.org/10.7567/JJAP.55.10TC04.
- [39] Y. Yoneda, D. Fu, S. Kohara, Local structure analysis of NaNbO<sub>3</sub>, J. Phys. Conf. 502 (1) (2014) 012022, https://doi.org/10.1088/1742-6596/502/1/012022, 2014/ 04/19
- [40] K. Wei, J. Duan, G. Li, H. Yu, H. Qi, H. Li, Novel NaNbO3-based relaxors featuring ultrahigh energy storage performance, J. Alloys Compd. 994 (2024) 174710.
- [41] R. Shi, et al., A novel lead-free NaNbO<sub>3</sub>-Bi(Zn<sub>0.5</sub>Ti<sub>0.5</sub>)O<sub>3</sub> ceramics system for energy storage application with excellent stability, J. Alloys Compd. 815 (2020) 152356, https://doi.org/10.1016/J.JALLCOM.2019.152356, 152356, 2020/1//.
- [42] J. Ma, Y. Lin, H. Yang, J. Tian, Achieved high energy storage property and power density in NaNbO<sub>3</sub>-Bi(Sn<sub>0.5</sub>Ni<sub>0.5</sub>)O<sub>3</sub> ceramics, J. Alloys Compd. 868 (2021) 159206, https://doi.org/10.1016/J.JALLCOM.2021.159206, 159206, 2021/7//.

- [43] Q. Zheng, et al., Ultrahigh breakdown strength of NaNbO<sub>3</sub>-based dielectric ceramics for high-voltage capacitor application, J. Am. Ceram. Soc. 107 (8) (2024)
- 5490-5501, https://doi.org/10.1111/jace.19827.
   [44] Y. Fan, Z. Zhou, R. Liang, X. Dong, Designing novel lead-free NaNbO<sub>3</sub>-based ceramic with superior comprehensive energy storage and discharge properties for dielectric capacitor applications via relaxor strategy, J. Eur. Ceram. Soc. 39 (15)
- (2019/12/01/2019) 4770–4777, https://doi.org/10.1016/j. jeurceramsoc.2019.07.021.
- [45] C. Sun, et al., Simultaneously with large energy density and high efficiency achieved in NaNbO<sub>3</sub>-based relaxor ferroelectric ceramics, J. Eur. Ceram. Soc. 41 (3) (2021/03/01/2021) 1891–1903, https://doi.org/10.1016/j. jeurceramsoc.2020.10.049.